# Modeling grain boundary and surface segregation in multicomponent high-entropy alloys

Paul Wynblatt[1,*] and Dominique Chatain[2]
[1]Department of Materials Science and Engineering, Carnegie Mellon University, Pittsburgh, Pennsylvania 15213, USA
[2]Aix-Marseille Univ, CNRS, CINaM, Marseille, France

(Received 10 April 2019; published 28 May 2019)

Grain boundary (GB) and surface segregation have been studied by computer simulations in the so-called Cantor alloy: $Co_{20}Ni_{20}Cr_{20}Fe_{20}Mn_{20}$. Monte Carlo, molecular dynamics, as well as lattice statics methods, using second nearest-neighbor modified embedded atom method potentials, have been applied sequentially in order to equilibrate the alloy. Simulations of GB segregation showed that Cr segregates most strongly, and is accompanied by weak Mn segregation. In contrast, in the case of surface segregation, Mn segregates most strongly to the outermost surface atom plane. However, when adsorption is measured as the integrated excess of the components over a 4-atom-layer region adjacent to the surface, Cr again emerges as the dominant segregant. A mass balance model has also been applied to the results of the segregation behavior, in order to estimate the potential for depletion of the bulk alloy composition due to segregation at GBs. It is found that significant depletion of bulk composition can occur if the alloy grain size falls below about 100 nm.

DOI: 10.1103/PhysRevMaterials.3.054004

## I. INTRODUCTION

Alloys consisting of five or more components in equiatomic proportions have recently attracted significant attention [1,2]. They have often been referred to as high-entropy alloys (HEA) [3] because their configurational entropy (or entropy of mixing) is maximized when all the components are present at the same atom fraction. Originally, the high configurational entropy was considered to favor the formation of random solid solutions, rather than possibly brittle intermetallic phases, thereby promising to achieve more attractive mechanical properties. However, an increasing number of recent studies, in which experiments and calculations have been combined, indicates a trend to show that the enthalpy of mixing also plays a major role in stabilizing single phases in these multicomponent alloys. In addition, it has been shown that reliable modeling of the structure and the thermodynamics of complex alloys is required in order to understand their special properties [4].

The principal objective of this paper is to investigate interfacial segregation (adsorption) phenomena, with particular emphasis on grain boundary (GB) segregation, while also taking a more cursory look at surface segregation. Interfacial segregation effects may potentially be interesting from at least two perspectives: (a) the most detailed previous studies of segregation in multicomponent systems [5–8] have generally been limited to ternary alloy systems and it might therefore be interesting to determine whether any new phenomena arise with increasing numbers of components, and (b) in polycrystalline thin films of small grain size, it is conceivable that strong grain boundary segregation of one (or more) components could sufficiently deplete the segregating species from the "bulk" of the film, that it might lead to the formation of new bulk phases.

We have chosen the so-called Cantor alloy, $Co_{20}Ni_{20}Cr_{20}Fe_{20}Mn_{20}$, for this study, because it has received significant experimental investigation (see, for example, Refs. [9–15]). In particular, Li *et al.* [9] have reported on atom probe investigations of this alloy, produced by combinatorial experimental procedures, which have identified elements that segregate to GBs at low temperatures. In addition, a consistent set of "second nearest-neighbor modified embedded atom method" (2NN MEAM) potentials for this particular combination of elements has recently become available [16] thereby making the Cantor alloy a convenient example for study by atomistic computer simulation.

This paper provides a first investigation of interfaces in complex polycrystalline alloys, which will undoubtedly contribute to improved understanding of their interesting behavior.

## II. COMPUTATIONAL APPROACH

Modeling was conducted by a combination of Monte Carlo (MC), molecular dynamics (MD) and lattice statics (LS) types of simulations, employing the LAMMPS code [17–19] in conjunction with 2NN MEAM potentials [16]. These MEAM potentials have extended the applicability of the widely used embedded atom method (EAM) potentials, beyond FCC metallic systems, to other crystal structures commonly encountered in metals and alloys.

The computation cell for modeling of surface segregation consisted of 4000 atoms of the five components randomly distributed on FCC crystal sites, arranged in the shape of a cube, with periodic boundary conditions in the $x$ and $y$ directions, and terminated by two (001) surfaces normal to the $z$ direction [see Fig. 1(a)].

The modeling of GB segregation was performed on computation cells consisting of 8320 randomly distributed atoms of the five species arranged in the shape of a rectangular parallelepiped, and occupying FCC crystal sites. Periodic

*pw01@andrew.cmu.edu

 

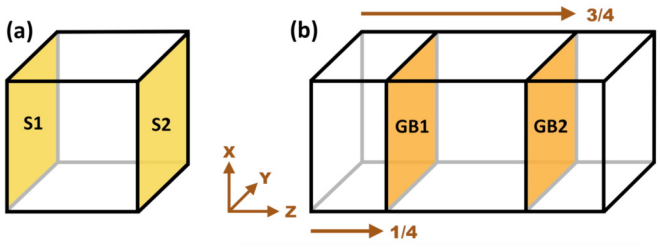


FIG. 1. Schematic of the computational cells; (a) a cube with two {100} surfaces, S1 and S2, and (b) a three segment rectangular parallelepiped with 2 ⟨100⟩ twist GBs, GB1, and GB2.

boundary conditions were applied along all three axes. Two GBs lying perpendicular to the $z$ axis were located at ∼0.25 and 0.75 of the $z$ dimension [see Fig. 1(b)], with the $z$ direction running parallel to the [001] crystallographic direction and consisting of 40 (002) planes. The GBs were constructed by rotating the central segment of the computation cell clockwise about the $z$ axis by an angle of 11.31°, and rotating the other two segments of the cell counterclockwise by the same angle, to produce two "pseudo Σ13" GBs.

It is useful to explain what we mean by pseudo Σ13 GBs. Let us recall that a FCC crystal may be viewed as consisting of two types of {100} planes stacked in ABAB … sequence. In a given crystal, the A and B planes normal to the [001] axis are related by a translation along either the [100] or the [010] direction by a distance of half a lattice constant. A conventional Σ13 coincidence site lattice (CSL) GB may be created between two crystals terminated on {100} FCC planes, and requires that both planes be either A-type or B-type {100} planes, such that upon twisting one crystal by 22.62° with respect to the other about a ⟨100⟩ type direction, one site in 13 on one GB terminating plane will have in-plane ($x$, $y$) coordinates that coincide with those of a corresponding site on the opposite terminating plane. The interface structure of this type of GB is shown in Fig. 2(a) for a case where two crystals terminated on their (001) A-planes have been twisted about their common [001] normal. In Fig. 2(b), we have formed the GB by a relative angular twist of 22.62° of one crystal terminated by a (001) A-type plane with respect to another (second) crystal terminated by a (001) B-type plane. The result is that there are no coincident atom sites on the terminating planes. However, it is still possible to apply periodic boundary conditions in the $x$ and y directions, something that is not possible for general non-CSL GBs. Finally, Fig. 2(c) shows the results of relaxing (i.e., equilibrating by LS) the GB structure of Fig. 2(b) in the Cantor alloy [the different components are not identified in Fig. 2(c)], and illustrates that the GB no longer displays any obvious periodicities.

It has been shown previously that a systematic removal of atoms from a GB plays an important role in identifying the GB configurations of minimum energy [20]. Thus, in order to ensure that the GBs are in compositional equilibrium with their surroundings (something that is necessary in the study of an equilibrium phenomenon such as interfacial segregation), GBs with closely spaced atoms residing at coincident sites would likely require the removal of many atoms in order to reach their lowest interfacial energy. This could tend to make CSL GBs atypical as they might display relatively more free volume than general high-angle GBs. However, we have computed the energy of the pseudo Σ13 GB used here, as a function the number of high-energy atoms removed and find that the minimum energy GB is obtained when no atoms are removed from the boundary region.

GB segregation was computed at four temperatures, from 1000 to 1300 K at 100 K intervals, whereas surface segregation was only calculated at 1100 K. 1000 K was selected as the lowest temperature for simulations as there is evidence to suggest that the FCC phase in the Cantor alloy becomes unstable below that temperature [21,22]. As a first step in all calculations, the computation cells, consisting of equal numbers of atoms of the five species distributed at random, were relaxed by LS. The cells were then subjected to a certain number of cycles, each of which included MC, MD and LS modeling, in sequence. For the MC segment of the cycle, a canonical simulation was used, in which only randomly selected atom exchanges within the computation cell were

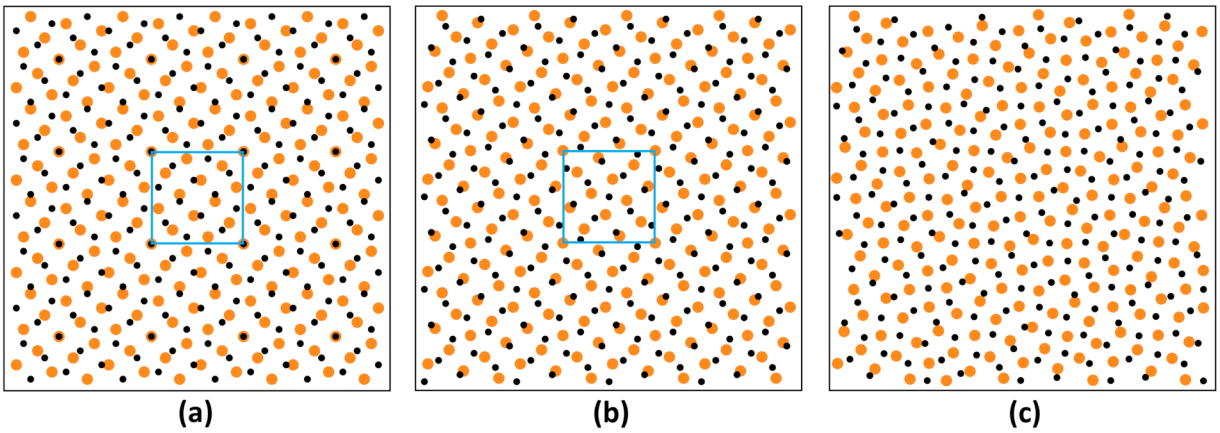


FIG. 2. Superposition of the two terminating (001) GB planes colored orange (large symbols) and black (small symbols), respectively, for (a) a conventional Σ13 GB, where the blue square identifies the interfacial unit cell with corners on coincident sites; (b) a "pseudo Σ13" GB; here no coincidences are present, but the structure is periodic and the blue square shows that the interfacial unit cell is of the same size as that of (a); and (c) a "pseudo Σ13" GB with the five Cantor alloy components distributed randomly on the two terminating GB planes, shown after relaxation by LS; in this case no obvious structural periodicity is observed, although periodic boundary conditions still apply.

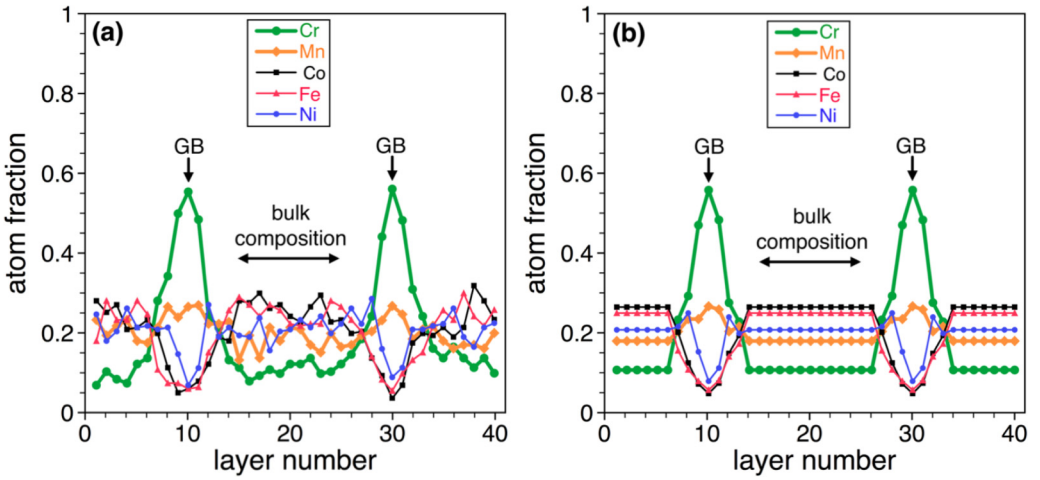


FIG. 3. Example of GB composition profile after equilibration at 1200 K. (a) Atom fraction profile of all components across the computation cell, calculated at each (002) plane. The location of the 2 GBs is indicated, as is the region over which the average bulk composition was computed. (b) Averaged composition profile, see text.

allowed, so as to maintain a fixed average overall equiatomic composition. This approach allows investigation of possible changes in bulk composition resulting from the segregation of certain species to either type of interface. The MC segment of the computations involved 45 000 attempted MC swaps of each possible pair of components. The percentage of successful attempted MC swaps was dependent on the chemical types of the pair of atoms selected for swapping, as well as on the temperature, and averaged from about 38% at 1000 K, to 54% at 1300 K. MC was followed by MD at the same temperature as MC, and involved two stages. The temperature was first gradually raised to the desired temperature over a period of about 12 picoseconds, and then equilibrated for about 12 more picoseconds to allow for positional equilibration. The final stage of each sequence involved LS relaxation at a temperature of 0 K. This is useful, as it allows an evaluation of the change in potential energy which results from the compositional redistribution that takes place during MC modeling. In our MD modeling we noticed no compositional redistribution of atoms on sites. The present MC-MD-LS cycles produced faster equilibration than other possible sequences. Ten such cycles were sufficient for equilibration at all temperatures.

## III. RESULTS

### A. Grain boundary segregation

Figure 3(a) is a typical result of the raw data obtained for the plane-by-plane composition profile along the $z$ direction (perpendicular to the GBs), after ten computation cycles at a temperature of 1200 K. It is clear that Cr segregates strongly to the GBs, the locations of which are indicated by arrows in the figure. In the GB regions there is also a clear deficiency of Co, Fe, and Ni, but Mn is present at a somewhat higher than its initial average bulk atom fraction of 20%. A central 10-atom-layer region is indicated by a double arrow labeled "bulk composition". This part of the profile was selected to compute the bulk composition, as the average atom fraction of all components over that region. The two GBs have been assumed to extend over a total of 7-atom layers each, a region which covers essentially all of the composition excursion associated with the GBs. Figure 3(b) shows the same data after all regions outside the 7-atom-layer GB regions have been assigned the average bulk composition, and the compositions of each of the 7-atom layers of the 2 GBs have been averaged. Note that the odd number of planes (7-layer width) that make up the composition excursion around the GB is related to the asymmetry of the pseudo Σ13 GB (a conventional Σ13 GB would presumably display a symmetric distribution of adsorbate as seen in Ref. [23]).

Figures 3(a) and 3(b) also show that the Cr atom fraction profile, which is highest in the GB regions, is also the lowest in the region from which bulk concentration is computed, indicating bulk depletion of Cr due to its strong segregation to the GBs. Conversely, the components that are strongly repelled from the GB regions (Co and Fe) are those with the highest concentrations in the bulk region.

A summary of the results over the whole range of temperatures investigated is shown in Fig. 4. Figure 4(a) gives the GB adsorption, reported as the sum of the excess atom fraction of each component, in the 7-atom-layer GB region, above its average bulk atom fraction. Figure 4(b) reports the corresponding change in average bulk composition. Figure 4 confirms the trends displayed in Fig. 3 with respect to bulk concentration depletion or augmentation depending on GB segregation behavior. Note also, that as temperature increases the GB segregation of Cr (the primary segregant) decreases. This reduces the degree of bulk depletion, so that the average bulk atom fraction of Cr increases with increasing temperature. For the particular conditions of these computations (i.e., the effective grain size of our computation cell) the Cr bulk atom fraction can drop as low as 0.05, i.e. one quarter of its value prior to segregation.

### B. Surface segregation

The averaged surface segregation profile obtained after equilibration at 1100 K is presented in Fig. 5. Several points are worthy of note. The element present at the highest

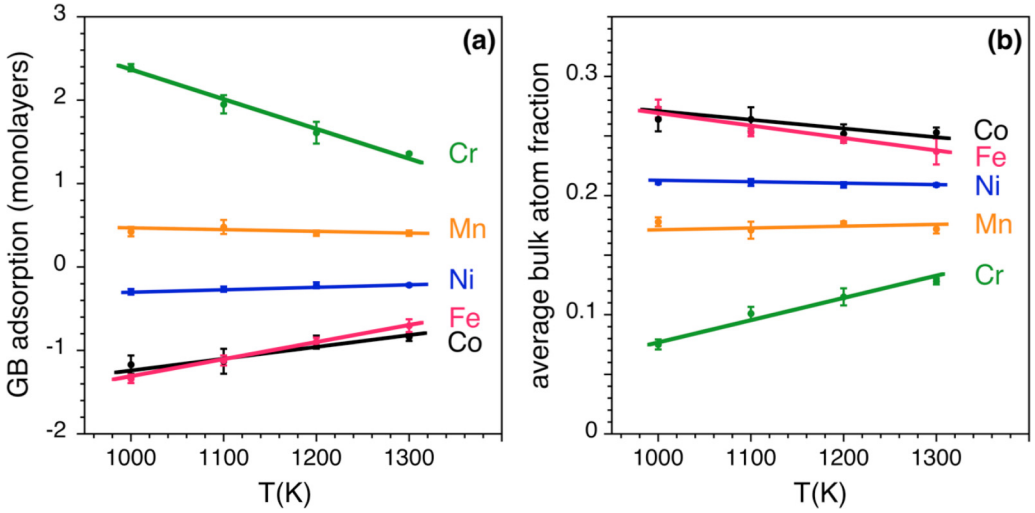


FIG. 4. (a) Plot of GB adsorption versus temperature for all five alloy components, where positive adsorption indicates excess and negative adsorption indicates deficiency of the component in relation to the average bulk composition. (b) Plot of the average bulk composition of all components as a function of temperature.

concentration in the outermost surface atom layer is Mn. However, the surface-related composition excursion, which is about 4-atom-layers wide, does not vary monotonically, and the total adsorption (i.e., the integrated surface excess over the bulk atom fraction computed from the 4-atom-layer surface region) is found to be larger for Cr (0.48 monolayers) than for Mn (0.28 monolayers).

## IV. DISCUSSION

### A. Driving forces for interfacial segregation

The basic forces that drive a given component to segregate to an interface are similar whether a system consists of two or more components. As was proposed some time ago [24], there are three terms that tend to drive interfacial segregation of a given component to an interface: (a) an interfacial energy term and (b) an alloy interaction term, both of which were suggested by Defay and Prigogine [25] for segregation to a liquid surface, and (c) an elastic solute strain energy term identified for interfaces in solids by McLean [26] as the strain energy associated with a solute atom in the bulk far from the interface that is relieved at the interface. All three of those terms were eventually combined into a single regular solution framework [24]. The relationship between the atom fraction of segregant in the interface, $x^i$, and its bulk atom fraction, $x^b$, in a two-component (A-B) system may be expressed as [24,27]

$$\frac{x^i}{1-x^i} = \frac{x^b}{1-x^b}\exp\left(-\frac{\Delta H_{\rm seg}}{RT}\right) \equiv \frac{x^b}{1-x^b}K, \qquad (1)$$

where the enthalpy of segregation $\Delta H_{\rm seg}$ is the driving force for segregation to the interface, $R$ is the gas constant, $T$ is the absolute temperature, and $K$ is generally referred to as the interfacial enrichment factor. Equation (1) merely provides a relationship between interfacial and bulk composition, without accounting for the mass balance constraints that would arise as a consequence of the current canonical MC modeling. $\Delta H_{\rm seg}$ is the quantity that may be written as the sum of the driving forces for segregation:

$$\Delta H_{\rm seg} = (\gamma_B - \gamma_A)\Omega + 2\omega_{AB}[z^l(x^b - x^i) + z^v(x^b - 0.5)] - F(M)\Delta r^2, \qquad (2)$$

where the first term is the interfacial energy term in which the $\gamma_i$ are the interfacial energies of the ith components and $\Omega$ is the molar area; the second term is the alloy interaction term which contains the regular solution constant, $\omega_{AB}$ (proportional to the enthalpy of mixing of the binary AB alloy), and $z^l$ and $z^v$ which are the numbers of bonds of an atom to neighbors that lie either within the same atom plane or in adjacent planes, respectively; and the third term is the elastic solute strain energy which consists of a function of elastic moduli, $F(M)$, and $\Delta r$, the difference in atomic radii between the segregating species and the bulk component.

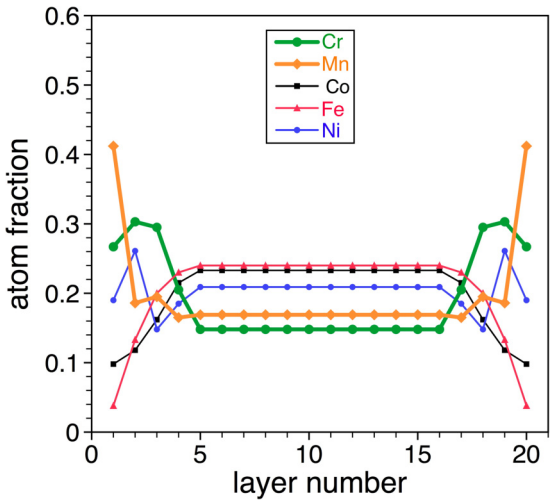


FIG. 5. Averaged composition profile, for an assumed 4-atom-layer surface region, obtained for surface segregation after equilibration at a temperature of 1100 K.

Important differences are known to exist between interfacial segregation in two-component systems versus systems with three or more components. Three-component systems display such effects as co-segregation and site competition, which were identified in the early work of segregation in ternary systems [5]. Site competition is a phenomenon in which two components that both display an attraction to the interface, but a mutually repulsive alloy interaction, will compete to occupy interface sites, with the component having the stronger affinity for the interface eventually driving the second component away. In contrast, co-segregation occurs when the segregation of the component that has a weaker interaction with the interface is also attracted to the component most strongly attracted to the interface; this type of combination enhances the interfacial segregation of the component with the weaker attraction to the interface (see, for example, Refs. [28,29]). Co-segregation tends to occur in systems with pairs of components that display either long or short-range ordering tendencies, whereas site competition, which requires pairs of components that display repulsive interactions, occurs in the presence of components that exhibit a tendency to cluster [24].

Although site competition and co-segregation phenomena were first identified in ternary alloy systems there is no reason why these phenomena need to be restricted to three-component systems. For example, co-segregation is often characterized by oscillatory composition profiles in the near-interface segregated region, as displayed here for example by Cr and Ni in Fig. 5.

Another interesting observation pointed out above is the qualitative difference between the composition profiles of a pseudo $\Sigma 13$ GB and a {100} surface. The surface segregation profile of Fig. 5 shows that Mn is the element with the highest concentration at the outermost surface layer, whereas the GB segregation profile of Fig. 3(b) is dominated by Cr segregation. Whether a component is present in excess at an interface is determined by the sign of the sum of the three terms that make up $\Delta H_{\text{seg}}$ in Eq. (2), with a net negative sign of $\Delta H_{\text{seg}}$ being favorable for segregation. In the case of segregation in a two-component system, the probability of a sign change in $\Delta H_{\text{seg}}$ between GB and surface segregation is rather small. But the results of Figs. 3(b) and 5 indicate that when multiple components are present, the interplay between the factors that enter into $\Delta H_{\text{seg}}$ may lead to unexpected results, as explained at greater length below.

Of the three principal factors mentioned above that enter into the enthalpy of segregation, the interfacial energy, which reflects the number of broken bonds of atoms in the interface, plays a larger role in the case of surface segregation than in GB segregation. This is because a large fraction of the broken bonds present on one side of a GB are reconnected to atoms on the other side of the GB, i.e. to atoms on the terminating plane of the opposite crystal. The resulting decrease in the number of broken bonds lowers the GB energy in comparison to the surface energy by about a factor of three.

Table I gives the (100) surface energies of all five pure components of the Cantor alloy, in the FCC structure, as computed by means of the present MEAM potentials at a temperature of 0 K. In addition, the table provides reported surface energies of the pure solid elements, at their melting points, as determined from the experimental liquid-vapor surface energies by the application of a semi-empirical scheme [30]. Both sets of values indicate that Mn displays the lowest surface energy, i.e., replacing any surface atom of the other four components by a Mn atom will decrease the surface energy. It is therefore not surprising that Mn is the majority segregating component at the very surface of the Cantor alloy.

TABLE I. Computed and reported surface energies ($\text{mJ.m}^{-2}$) of the five Cantor alloy elements.

| Elements | Present computations | Reported literature values[a] |
|---|---|---|
| Co | 2117 | 2218 |
| Ni | 1938 | 2080 |
| Cr | 2122 | 2006 |
| Fe | 2371 | 2123 |
| Mn | 1600 | 1298 |

[a]Reference [30].

Another factor in the driving force for segregation is the strain energy associated with a given segregating atom in the bulk of the alloy due to size differences with the average matrix atom. Table II provides the values of the atomic radii for the five elements of interest, as computed here in the FCC structure, as well as the averaged atomic radius of the Cantor alloy. Referring to Eq. (2), it can be seen that the elastic strain energy (computed under the assumption of linear elasticity) depends on the square of the radius difference between a given component and the averaged alloy radius. However, segregation experiments have shown [31,32] that the strain energy only obeys the linear elastic theory for segregating atoms with radii that are larger than the matrix average, i.e., for elements that show a positive difference in the third column of Table II. Thus the elastic strain energy contribution would tend to favor the segregation of Mn most strongly, with Cr being in second place.

Since two of the three driving forces for interfacial segregation favor Mn, one must conclude that the greater segregation driving force displayed by Cr at GBs must come from the third term in the driving force, namely the "alloy interaction" term. That part of the driving force is not trivial to evaluate in a five component system because, as can be seen from Eq. (2),

TABLE II. Computed atomic radii of the five Cantor alloy elements as well as the averaged value for the Cantor alloy in the FCC structure.

| Elements | Computed atomic radii (nm) | Difference in atomic radii (nm) $r_{\text{element}} - r_{\text{Cantor}}$ |
|---|---|---|
| Co | 0.1250 | −0.0021 |
| Ni | 0.1245 | −0.0026 |
| Cr | 0.1290 | 0.0019 |
| Fe | 0.1277 | 0.0006 |
| Mn | 0.1303 | 0.0032 |
| Cantor alloy | 0.1271 | – |

it depends on the regular solution constant in the case of a binary alloy. In a five component system, the single regular solution constant of Eq. (2) is replaced by a linear combination of 10 different $\omega_{ij}$ $(i, j = 1, 5, i \neq j)$. Furthermore, each $\omega_{ij}$ depends not only on the bond energy $\epsilon_{ij}$ but also on $\epsilon_{ii}$ and $\epsilon_{jj}$, i.e., $\omega_{ij} = \epsilon_{ij} - 0.5(\epsilon_{ii} + \epsilon_{jj})$. However, Figs. 3(b) and 5, which provide the composition profile across a segregated GB and surface, respectively, provide a clue as to the relative importance of these bond energies. The Mn interfacial excess in Fig. 5 extends to only a single atom layer, whereas the Cr excess at the GBs of Fig. 3(b) extends to three-atom layers on either side of the GB. Thus the part of the driving force that leads Cr excess to supercede the Mn excess at the (100) surface is apparently a stronger affinity of Cr for Cr than that of Mn for Mn. If that is the case, then once some Cr has segregated to an interface, more Cr tends to join, whereas Mn does not attract more Mn. This inference is supported by estimates we have made of the affinity of Cr for Cr and of Mn for Mn given below.

Consider the Cr-Cr case. We have determined the percentage change in the number of Cr-Cr bonds that are present in the bulk of the Cantor alloy at 1200 K, compared with the number of Cr-Cr bonds that would be present in a random solid solution [at the observed bulk composition reported in Fig. 4(b)]. That change is an increase of 48%. The computed value of the percentage difference in the number of Mn-Mn bonds between the equilibrated alloy at 1200 K and the random alloy is −4%. This clearly implies that greater numbers of additional Cr atoms are likely to congregate around a Cr segregated interface than Mn atoms around a Mn segregated interface. Thus, although Mn segregation might benefit from more favorable surface energy and strain energy driving force terms, Cr appears to have a more favorable alloy interaction term. This term is a stronger contributory to the driving force for GB segregation than for surface segregation, because most of the bonds that are broken at a surface, are replaced by bonds from one GB terminating plane to the terminating plane on the other side of the GB.

### B. Bulk and interfacial component depletion due to interfacial segregation

A model was developed some time ago [33] to examine the effects of catalyst particle size on the relation between surface and bulk compositions that would result from surface segregation in two-component catalyst particles, under conditions of fixed overall composition. Interest in that issue stemmed from the possibility of using alloys containing modest bulk concentrations of a catalytically active component, and exploiting surface segregation to enrich the surface in costly catalytically active species. We have seen here that when a given component segregates to interfaces its bulk concentration can decrease (because of the imposed mass balance constraints), and as bulk concentration decreases, so will the interfacial concentration [by Eq. (1), which determines the relation between interfacial and bulk compositions]. Thus it was deemed important to identify the particle size at which some gain of surface active species would be retained. The model was tested against measurements of surface segregation in samples of a Ni-1at%Pd alloy prepared with several different particle sizes [33], and it correctly predicted that both surface and bulk concentrations of Pd would begin to decrease at particle sizes below about 100 nm. Although that model is not entirely suitable for evaluating the behavior of a five-component alloy, we have applied it here to provide a rough estimate of the relationship between interfacial and bulk compositions and grain size in the Cantor alloy, under the following assumptions. (1) The Cantor alloy is approximated by a $Cr_{20}X_{80}$ pseudobinary alloy. (2) The overall atom fraction of Cr is fixed at 0.2. We choose a temperature such that in the limit of an infinite grain size (i.e., a negligible fraction of interface sites) the atom fraction in the segregated GB is represented by $x^i = 0.5$. Fixing $x^i$ also fixes $\Delta H_{\text{seg}}/RT$ and $K$ in Eq. (1), which remain constant when the grain size changes. (3) Grains are assumed to adopt a cubic shape bounded by GBs that all display the same segregation behavior. (4) Any changes resulting from decrease in grain size are assumed to result from mass balance considerations (i.e., capillarity effects are ignored).

For an average cubic grain of edge length $r$, the grain volume is $V = r^3$, and its grain boundary area is $A = 3r^2$. This accounts for the fact that each GB is shared by two cubes and that each cube has 6 neighbors. The volume of the GBs is taken to be $A\Delta r$, where the boundary width, $\Delta r$, is estimated to be twice the average diameter of an atom in the Cantor alloy (0.508 nm). We also define the ratio, $D$, of the number of atomic GB sites to the total number of atomic sites in a grain as being approximately equal to their volume ratio:

$$D = \frac{A\Delta r}{V} = \frac{3r^2\Delta r}{r^3} = \frac{3\Delta r}{r}. \tag{3}$$

It is also useful to define a mass balance condition such that the sum of the numbers of atoms of segregant in the GB, plus those in the bulk, remains equal to the total number of atoms of the segregating species in the system. If the number of atoms is taken to be proportional to volume, then

$$x^i A\Delta r + x^b(V - A\Delta r) = \bar{x}V,$$

where $\bar{x}$ is the average atom fraction of 0.2. Dividing through by $V$ we have

$$x^i D + x^b(1 - D) - \bar{x} = 0. \tag{4}$$

Finally, substituting Eq. (1) into Eq. (4), and eliminating $x^b$, we obtain a quadratic equation in $x^i$:

$$D(1 - K)(x^i)^2 + [DK + 1 - D - \bar{x}(1 - K)]x^i - \bar{x}K = 0. \tag{5}$$

$x^i$ can be obtained by solving Eq. (5), and may then be used to compute the corresponding value of $x^b$ from Eq. (1). The resulting estimated variations of $x^i$ and $x^b$ with grain size are displayed in Fig. 6, which indicates that the effects of grain size change on both the grain boundary and the bulk grain compositions become significant only for grain sizes below about 100 nm.

### C. Agreement with experiment

Li *et al.* [9] have reported composition profile measurements by atom probe tomography (APT) on Cantor alloy thin films that provide some information on GB segregation.

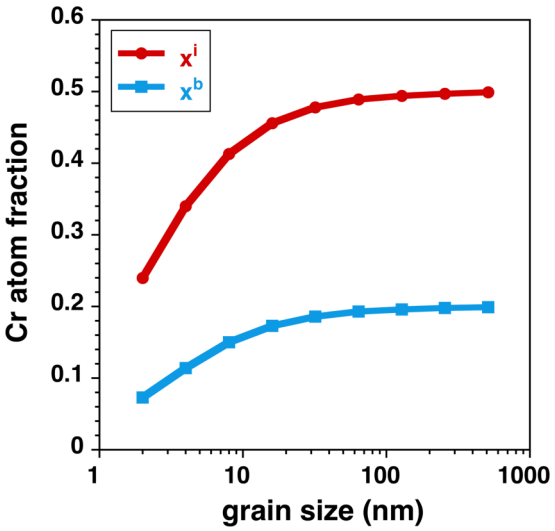


FIG. 6. Variation of Cr atom fraction in the GB ($x^i$, curve in red with round symbols) and in the bulk of the grain ($x^b$, curve in blue with square symbols) which results from mass balance considerations, plotted as a function of grain size.

The Cantor alloy, deposited on Si tips, and heat treated for 1 to 2 hours at temperatures ranging from 423 to 623 K, was then gradually field evaporated and analyzed. Even after annealing at temperatures as low as 423 K, the authors saw evidence of Ni and Mn segregated to the grain boundaries. By 573 K, Cr GB segregation was also identified. However, on reaching this temperature they also saw evidence for the formation of several new phases formed by decomposition of the Cantor alloy into a Cr-rich BCC phase, a Ni-rich $L1_0$ phase, a Cr-rich $\sigma$ phase, and an Fe-rich B2 phase, each of which has its own composition which departs from the (average) bulk composition of the alloy. Thus, it is difficult to make quantitative comparisons between those observations and the present results obtained at much higher temperatures, although there is qualitative agreement on the segregation of Mn and Cr to the GBs. This indirect agreement is the only currently available support for the reliability of the 2NN MEAM potentials [16] for predicting interfacial behavior.

### D. Impact on phase stability

Both modeling and experiment have shown that increasing Cr concentration beyond ∼20% tends to stabilize the BCC phase, which will then coexist with the FCC phase above about 1000 K [14,15]. Thus, as Cr is depleted from the bulk by segregation at GBs or surfaces, the FCC alloy will tend to remain even more stable. It is also important to emphasize that the 7-layer-thick Cr-rich GB region of Fig. 3 is not a phase but a segregated layer, i.e., a complexion [34,35]. The significant segregation observed at a pseudo $\Sigma 13$ GB will most likely also take place at other GBs, however the quantity segregated will vary from one GB to another since GB segregation is anisotropic [23]. The FCC Cr-rich regions located at the GBs could serve as seeds for the nucleation of Cr-rich $\sigma$ phase precipitates, which have been reported to occur in the Cantor alloy after annealing for up to 1000 h or 500 days at 973 K, respectively [21,22].

## V. SUMMARY

GB segregation has been studied in the Cantor alloy by computer simulation at temperatures ranging from 1000 to 1300 K. In addition, a more cursory investigation of surface segregation has been performed at 1100 K. Although Mn segregates most strongly to the outermost surface layer in the case of surface segregation, presumably because Mn has the lowest surface energy of all of the Cantor alloy components, the calculated Cr adsorption integrated over four surface atomic layers is larger than that of Mn. Cr also displays the strongest adsorption at GBs. These results have been interpreted in terms of the three principal driving forces for interfacial segregation: interfacial energy, alloy interaction and elastic strain energy due to atom size differences. The driving forces for surface segregation are different from those for GB segregation. While Mn surface segregation benefits from a favorable surface energy, and both Mn and Cr have elastic strain energies that favor interfacial segregation, Cr has a stronger alloy interaction. The present simulations have been conducted in a closed system, in order to assess whether interfacial segregation can deplete the bulk atom fraction of the segregating species, thereby leading to the possible formation of new phases. A simple model based on mass balance shows that significant bulk depletion of Cr can occur only if the grain size falls below 100 nm.

## ACKNOWLEDGMENTS

PW acknowledges with thanks use of the resources of the National Energy Research Scientific Computing Center (NERSC), a US Department of Energy Office of Science User Facility operated under Contract No. DE-AC02-05CH11231. DC wishes to acknowledge the French Agence Nationale de la Recherche for support of her research under grant ANR-16-CE92-0015 in the framework of the ANR-DFG project: Analysis of the Stability of High Entropy Alloys by Dewetting of Thin Films (AHEAD). Both authors also wish to thank other members of the AHEAD project, for fruitful discussions.

[1] B. Cantor, I. T. H. Chang, P. Knight, and A. J. B. Vincent, Mater. Sci. Eng. A **375–377**, 213 (2004).
[2] S. Ranganathan, Curr. Sci. **85**, 1404 (2003).
[3] J. W. Yeh, S. K. Chen, S. J. Lin, J. Y. Gan, T. S. Chin, and T. T. Shun, Adv. Eng. Mater. **6**, 299 (2004).
[4] M. Widom, J. Mater. Res. **33**, 2881 (2018).
[5] M. Guttmann and D. McLean, in *Interfacial Segregation*, edited by W. C. Johnson and J. M. Blakely (American Society for Metals, Metals Park, OH, 1979), pp. 261−348.

[6] M. A. Hoffmann and P. Wynblatt, Metall. Trans. A **20**, 215 (1989).
[7] M. A. Hoffmann and P. Wynblatt, Metall. Trans. A **22**, 1833 (1991).
[8] M. A. Hoffmann and P. Wynblatt, Metall. Trans. A **22**, 1841 (1991).
[9] Y. J. Li, A. Savan, A. Kostka, H. S. Stein, and A. Ludwig, Mater. Horiz. **5**, 86 (2018).
[10] C. Haase, F. Tang, and M. B. Wilms, Mater. Sci. Eng. A **688**, 180 (2017).
[11] Z. Li, C. C. Tasan, K. G. Pradeep, and D. Raabe, Acta Mater. **131**, 323 (2017).
[12] K. V. S. Thurston, B. Gludovatz, A. Hohenwarter, G. Laplanche, E. A. George, and R. O. Ritchie, Intermetallics **88**, 65 (2017).
[13] C. C. Koch, J. Mater. Res. **32**, 3435 (2017).
[14] G. Bracq, M. Laurent-Brocq, L. Perriere, R. Pires, J.-M. Joubert, and I. Guillot, Acta Mater. **128**, 327 (2017).
[15] W.-M. Choi, S. Jung, Y. H. Jo, S. Lee, and B.-J. Lee, Met. Mater. Int. **23**, 839 (2017).
[16] W.-M. Choi, Y. H. Jo, S. S. Sohn, S. Lee, and B.-J. Lee, npj Comput. Mater. **4**, 1 (2018).
[17] S. J. Plimpton, J. Comput. Phys. **117**, 1 (1995).
[18] http://lammps.sandia.gov/ (accessed March 2019).
[19] http://lammps.sandia.gov/workshops/Aug15/PDF/talk_Thompson1.pdf (accessed March 2019).
[20] S. von Alfthan, P. D. Haynes, K. Kaski, and A. P. Sutton, Phys. Rev. Lett. **96**, 055505 (2006).
[21] E. J. Pickering, R. Muñoz-Moreno, H. J. Stone, and N. G. Jones, Scripta Mater. **113**, 106 (2016).
[22] F. Otto, A. Dlouhý, K. G. Pradeep, M. Kubenova, D. Raabe, G. Eggeler, and E. P. George, Acta Mater. **112**, 40 (2016).
[23] P. Wynblatt, D. Chatain, and Y. Pang, J. Mater. Sci. **41**, 7760 (2006).
[24] P. Wynblatt and R. C. Ku, Surface Sci. **65**, 511 (1977).
[25] R. Defay, I. Prigogine, A. Bellmans, and D. A. Everett. *Surface Tension and Adsorption* (Wiley, New York, 1966), p. 158.
[26] D. McLean. *Grain Boundaries in Metals* (Oxford University Press, London, 1957).
[27] P. Wynblatt and D. Chatain, Metall. Mater. Trans. A **37**, 2595 (2006).
[28] W.-C. Cheng and P. Wynblatt, Surface Sci. **302**, 179 (1994).
[29] A. Landa, P. Wynblatt, A. Girshick, V. Vitek, A. Ruban, and H. Skriver, Acta Mater. **46**, 3027 (1998).
[30] W. R. Tyson and W. A. Miller, Surface Sci. **62**, 267 (1977).
[31] N. H. Tsai, G. M. Pound, and F. F. Abraham, J. Catal **50**, 200 (1977).
[32] M. P. Seah, J. Catal **57**, 450 (1979).
[33] D. O. Groomes and P. Wynblatt, Surface Sci. **160**, 475 (1985).
[34] M. Tang, W. C. Carter, and R. M. Cannon, Phys. Rev. B **73**, 024102 (2006).
[35] W. D. Kaplan, D. Chatain, P. Wynblatt, and W. C. Carter, J. Mater. Sci. **48**, 5681 (2013).